PCCP

PAPER

View Article Online
View Journal | View Issue

Cite this: *Phys. Chem. Chem. Phys.*, 2014, **16**, 1672

Carbon dioxide adsorption on a ZnO(10$\bar{1}$0) substrate studied by infrared reflection absorption spectroscopy

Maria Buchholz, Peter G. Weidler, Fabian Bebensee, Alexei Nefedov and Christof Wöll*

Received 3rd November 2013,
Accepted 19th November 2013

DOI: 10.1039/c3cp54643h

www.rsc.org/pccp

The adsorption of carbon dioxide on the mixed-terminated ZnO(10$\bar{1}$0) surface of a bulk single crystal was studied by UHV Infrared Reflection Absorption Spectroscopy (IRRAS). In contrast to metals, the classic surface selection rule for IRRAS does not apply to bulk oxide crystals, and hence vibrational bands can also be observed for s-polarized light. Although this fact substantially complicates data interpretation, a careful analysis allows for a direct determination of the adsorbate geometry. Here, we demonstrate the huge potential of IR-spectroscopy for investigations on oxide single crystal surfaces by considering all three components of the incident polarized light separately. We find that the tridentate (surface) carbonate is aligned along the [0001] direction. A comparison to data reported previously for CO_2 adsorbed on the surfaces of ZnO nanoparticles provides important insight into the role of defects in the surface chemistry of powder particles.

Introduction

The semiconducting and optical properties[1–3] of zinc oxide (ZnO) give rise to strong interest from the physics community in this material. However, the chemical properties of ZnO and especially its technological importance for application in heterogeneous catalysis outweigh those exploiting the physical properties of this material by far. ZnO plays a crucial role in heterogeneous catalysis, both as a support material[4] as well as the catalytically active component. Methanol synthesis is the industrially most important chemical process in use today for converting CO_2 to larger molecules. In this process, syngas ($CO/CO_2/H_2$) is reacted to yield methanol, one of the most important chemical products with a yearly production volume exceeding 24 billion gallons. ZnO is the key component of the catalyst ($ZnO/Cu/Al_2O_3$) used in this important process.[5] ZnO also plays a special role with regard to CO_2 activation, which is currently one of the most important topics in catalysis.[6] In previous work it has been demonstrated that CO_2 can be activated on zinc oxide single crystals as well as on zinc oxide powder particles even below room temperature.[7–9] Fundamental interest in CO_2 activation has motivated investigations of CO_2 interaction with various other model oxide surfaces, *e.g.* CaO,[10,11] MgO,[12] Cr_2O_3,[13,14] RuO_2,[15,16] PdO,[17] and not least TiO_2,[18–20] which shows potential for photoreduction of CO_2 to hydrocarbons or methanol. Especially the thorough investigation of the structure and dynamics of CO_2 on rutile TiO_2(110)-1 × 1 by Lin *et al.*[20] provides an excellent basis for comparison to the findings reported in the present study, as it is one of the few publications reporting IRRAS data for CO_2 adsorbed on an oxide single crystal surface (along with a multitude of other surface science techniques).

Vibrational spectroscopy is of crucial importance for understanding the nature of the activated CO_2 species on the surface and its subsequent reactions. Unfortunately, high resolution infrared data are available up to now only for powder particles,[9] whereas for ZnO single crystals only high resolution electron energy loss spectroscopy (HREELS) data have been reported so far. The energy resolution of HREELS, however, is limited to about 100 cm^{-1}, which is clearly too low to resolve the different carbonate species observed by IR spectroscopy after exposing ZnO powders to CO_2.[7,9] While the application of IR spectroscopy to powders is rather straightforward, acquisition of IRRAS-data for oxide single crystals presents a formidable task owing to the low reflectivity of these materials for IR light.[21] In the case of ZnO, no previous infrared reflection absorption (IRRAS) study on clean single crystal surfaces has been reported. In a previous study, Thornton *et al.*[22] reported IR-spectra of CO adsorbed on ZnO(000$\bar{1}$) supported Cu particles revealing the typical stretch frequency for CO adsorbed on Cu-surfaces. Schott *et al.*,[23] on the other hand, reported IR-spectra of CO adsorbed on thin ZnO layers grown on a (111)-oriented brass single crystal.

Institut für Funktionelle Grenzflächen, Karlsruher Institut für Technologie, 76021 Karlsruhe, Germany. E-mail: christof.woell@kit.edu; Web: www.ifg.kit.edu; Fax: +49-721-608-2-3478; Tel: +49-721-608-2-3934

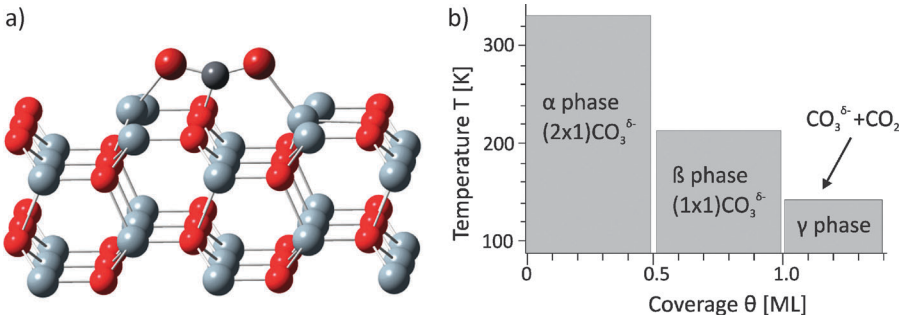

Fig. 1 (a) Ball-stick model of CO_2 adsorbed on ZnO(10$\bar{1}$0) (color code: red – oxygen, grey – titanium, black – carbon); (b) phase diagram of CO_2 on ZnO(10$\bar{1}$0) derived from TDS.[7]

In the present study, we report high-resolution IR-data for a carbonate species resulting from exposure of a (macroscopic) single crystal ZnO(10$\bar{1}$0) to CO_2.

The surface structure of ZnO has been studied in considerable detail during the last few decades.[24] Contrary to the polar surfaces, ZnO(0001) and ZnO(000$\bar{1}$), the ZnO(10$\bar{1}$0) surface is mixed-terminated; it consists of Zn–O pairs (see Fig. 1a), where both Zn and O atoms are threefold coordinated. The mixed-terminated surface does not exhibit an electrostatic instability like the two polar surfaces.[24]

The adsorption of CO_2 on ZnO(10$\bar{1}$0) has been studied previously with other techniques and it was found to result in the formation of a carbonate species.[7,12–14,24–26] In contrast to the carbonate bidentate structure proposed by Thornton *et al.*,[26] a recent combined experimental and theoretical effort demonstrated that a carbonate tridentate species is present on the surface.[7,24,25] Using helium atom scattering (HAS), a (1×1) and (2×1)-adsorbate phase could be identified when the ZnO(10$\bar{1}$0) surface was exposed to CO_2 at below room temperature. A thermodynamic analysis based on precise quantum chemical calculations using density functional theory (DFT) was used to construct the phase diagram shown in Fig. 1b. In the temperature regime from 95 K to 325 K and coverages of up to 0.5 ML, a (2×1) CO_3^{2-}-phase exists. In addition to this α-phase, a second, more densely packed β-phase corresponding to a (1×1) CO_3^{2-} layer was observed in the coverage regime from 0.5 ML to 1 ML and at temperatures between 95 K and 200 K. The γ-phase consists of a mixture of CO_3^{2-} and physisorbed CO_2 and forms above 1 ML coverage at temperatures between 95 K and 125 K. HREELS, X-ray photoelectron spectroscopy (XPS) and near edge X-ray absorption fine structure (NEXAFS) spectroscopy studies confirmed these findings.[25] HREELS measurements[7] on ZnO(10$\bar{1}$0) showed two types of carboxylate vibrations, a symmetric one at 1340 cm^{-1} and an asymmetric one at 1617 cm^{-1}. In these data, also the asymmetric CO_2 stretch vibration at 2355 cm^{-1} was detected.[7]

In the following we will analyze the high resolution IR-data recorded in the context of this study for s- and p-polarized light incident along two different azimuths and relate the results to the findings reported in the above mentioned previous studies. In order to aid the interpretation of our experimental data, we have carried out a simulation of the rather complex variation of IR-band intensities with polarization and the incidence angle following the approach proposed by Mielczarski *et al.*[27]

Experimental

All experimental results reported here were obtained using a novel advanced UHV-FTIR-apparatus (Prevac, Rogów, Poland), where a state-of-the-art FTIR spectrometer (Bruker Vertex 80v, Bruker Optics, Ettlingen, Germany) is directly coupled to an UHV chamber. This chamber is part of a larger, multi-technique UHV system allowing for a comprehensive characterization of samples. The apparatus is sufficiently flexible to change the optical path geometry from grazing incidence to transmission, thus also allowing for measurements on oxide powder samples.[28]

The ZnO(10$\bar{1}$0) single crystal (Crystec, Berlin, Germany) was cleaned by a sequence of sputtering (1.5 kV, 6 mA, 3×10^{-6} mbar Ar, 10 min) and annealing (800 K, 10 min) cycles. LEED was used to check the structural quality of the substrate – IRRAS measurements were only conducted after a well-defined (1×1) LEED pattern was obtained. Additionally, XPS measurements were performed to ensure sample cleanliness. In agreement with previous work, the Zn $2p_{3/2}$ and the O 1s peaks were observed at binding energies of 1021.8 eV and at 530.7 eV, respectively.[29]

Exposure to CO_2 (purity 99.995 vol%, Air Liquide, Düsseldorf, Germany) at sample temperatures typically below 100 K was carried out by backfilling the IR chamber up to 10^{-8} mbar. All IRRAS data recorded for the adsorbate-covered ZnO(10$\bar{1}$0) substrates were corrected by subtracting a background spectrum which was recorded prior to CO_2 exposure. During acquisition of the high resolution IR spectra, the pressure in the IR chamber remained below 2×10^{-10} mbar. All IRRAS data were recorded at grazing incidence (80°) with 2048 scans and a resolution of 4 cm^{-1} corresponding to an acquisition time of 9 minutes.

Results and discussion

Fig. 2 shows IRRA spectra recorded after exposing the sample at a temperature of 100 K to 1.5 L of CO_2. The LEED pattern recorded after adsorption of the CO_2 molecules showed the superstructure pattern typical for the (2×1)-phase of carboxylate

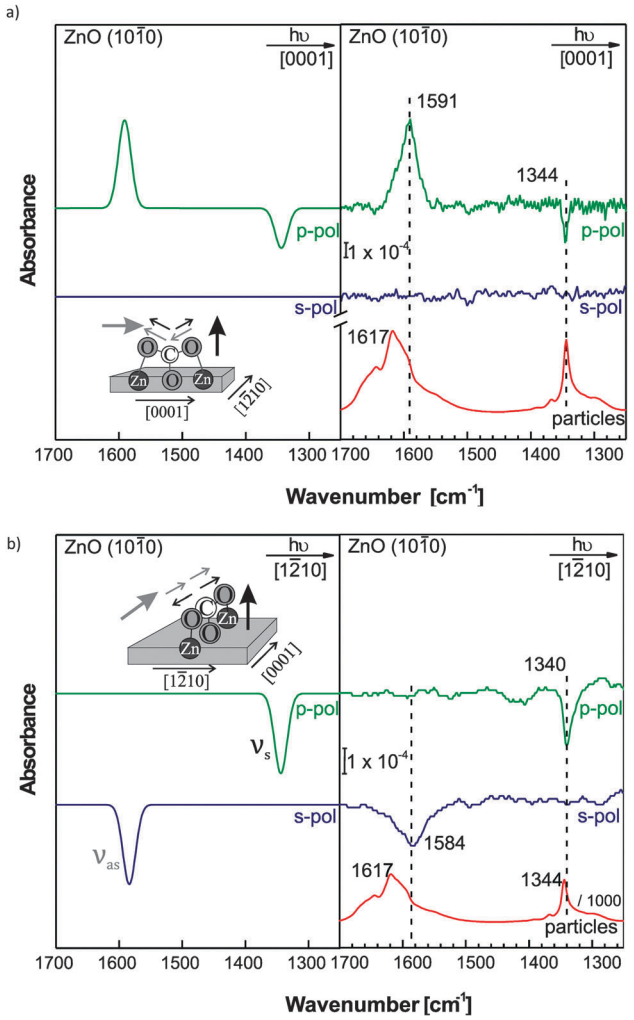

Fig. 2 Expected signals in IRRA spectra based on calculations (left panel) and experimental IRRA spectra of CO_2 on ZnO(10$\bar{1}$0) at a grazing incidence angle of 80° with s- and p-polarized light at 100 K (right panel). The sketch shows the orientation of the tridentate on the surface with the arrows indicating the movement during the vibrations. The big light and dark grey arrows indicate the orientation of the transition dipole moment of the vibrations. Together with the experimental data recorded for the ZnO(10$\bar{1}$0) single crystal, we show ZnO powder particle spectra.[9] (a) Incident beam along [0001] and (b) [1$\bar{2}$10] azimuth.

species on the surface (Fig. 3). IR spectra were recorded for both s- and p-polarized IR light incident along the [0001] and [1$\bar{2}$10] azimuthal directions. A complete data set for an exposure of 1.5 L is displayed in Fig. 2 together with the powder data reproduced from the paper by Noei *et al.*[9] In the spectrum recorded with p-polarized light incident along the [0001] azimuth, we observed one positive band at 1591 cm^{-1} and one negative band at 1344 cm^{-1}. The corresponding spectrum recorded with s-polarized light incident along the same direction is void of any features. Rather different results were obtained for the other high symmetry azimuth, *i.e.* the [1$\bar{2}$10] direction (see Fig. 2b). In this case, we observe distinct negative bands at 1589 cm^{-1} in the p-polarized spectrum and at 1340 cm^{-1} in the s-polarized spectrum (Fig. 2b).

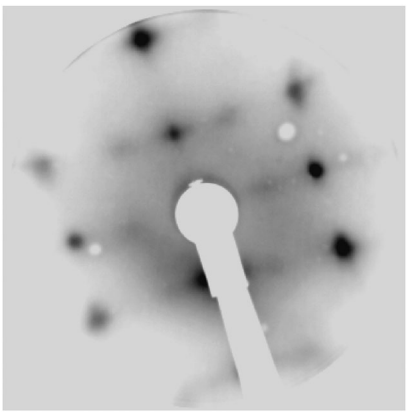

Fig. 3 LEED pattern of the (2 × 1)-CO_2 – phase on ZnO(10$\bar{1}$0) recorded after dosing 1.5 L at 100 K.

The experimental IRRAS-data shown in the right panels of Fig. 2 reveal that the analysis of IRRAS data recorded for the oxide single crystal surface is much more challenging than for metals. For metals, adsorbate vibrations couple only to p-polarized light (a result of the so-called surface selection rule[30,31]), absorption bands are always positive (*i.e.*, the reflectivity is reduced at the frequency of the corresponding adsorbate vibration), and only components of the vibrational transition dipole moments oriented perpendicular to the surface contribute to the IR-spectra. In the case of dielectric materials, the situation is more complicated: here, transition dipole moments oriented parallel to the surface can be probed, too. Hence, vibrations can be detected with s- and p-polarized (*i.e.*, the tangential component p_t) light. Finally, bands observed in the IR-spectra can be either positive or negative.

In order to aid the assignment of the features seen in the experimental IR data for the carbonate species on a ZnO(10$\bar{1}$0) surface, we will first present a prediction of the IR band signs and intensities using the following set of rules (spatial orientation of the vector-components is depicted in Fig. 4).

(1) s-Polarized light (*E*-vector E_s parallel to the surface)

– Only vibrations with a transition dipole moment exhibiting a component parallel to the surface and E_s can be observed.

– The sign of IR-bands observed in IRRAS for dielectric substrates is always negative.

(2) p-Polarized light

– The *E*-vector has to be decomposed into a tangential component, $E_{p,t}$, and a normal component, $E_{p,n}$.

– The sign of the signal arising from the two different components $E_{p,t}$ and $E_{p,n}$ is always opposite.

Applying these rules to the carbonate adsorption geometry proposed by Kotsis *et al.*[25] (Fig. 1a), where the carboxylate is adsorbed in an upright geometry with the backbone O–C–O-plane oriented along the [0001] direction and perpendicular to the substrate, yields the following predictions: as the transition dipole moment of the symmetric stretch vibration ν_s (TDM_s) is perpendicular to the surface, no contribution is expected in either azimuth for s-polarized light. The TDM of the asymmetric stretch vibrations ν_{as} (TDM_{as}) is oriented parallel to the

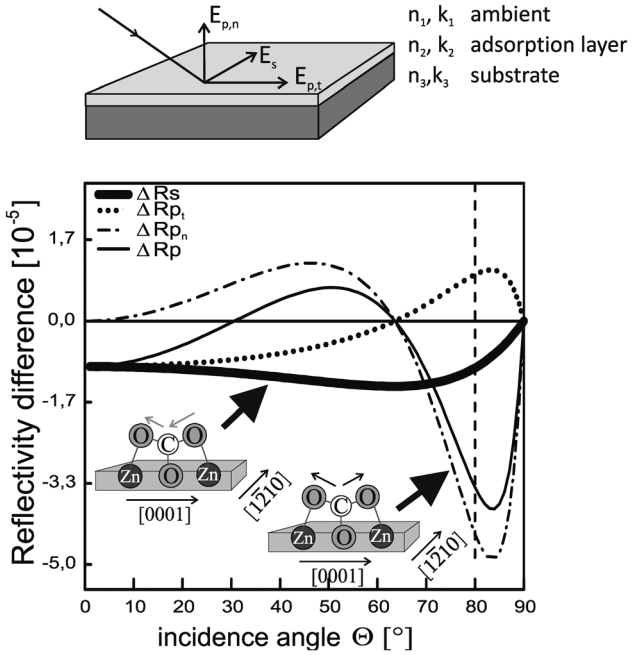

Fig. 4 Calculated reflectivity difference between the clean (R_0) and CO_2-covered ZnO(10$\bar{1}$0) substrate as a function of incidence angle for the p-polarized (n- and t-component (dashed lines) and sum (solid line)) and s-polarized (bold solid line) light at 1617 cm^{-1} (from ref. 7). Following optical constants were used: n_3 (substrate) = 2.013,[38] k_3 = 0, n_2 (CO_2) = 1.0310,[38] k_2 = 0.0001,[39] d_2 = 0.139 nm,[7] n_1 (vacuum) = 1, k_1 = 0. The insets show the asymmetric and symmetric carboxylate vibrations, which are excited by s- and p_n-light for light incident along the [1$\bar{2}$10] direction.

surface exactly along the [0001] direction, and thus we must expect a high intensity for s-polarized light incident along the [1$\bar{2}$10] azimuth and no intensity for incidence along the [0001] azimuth. For p-polarized light, a signal arising from the ν_s is expected for both azimuths due to coupling to the normal component of the E vector, $E_{p,n}$. An additional signal is expected from the ν_{as}, which can couple to the tangential component $E_{p,t}$ of p-polarized light incident along the [0001] azimuth, but not to p-polarized light incident along the [1$\bar{2}$10] azimuth. The results obtained by this heuristic approach are visualized in the left panels of Fig. 2. Note that we deliberately neglected any contributions from thermally occupied low-energy vibrations, *e.g.* frustrated rotations and translations (so-called dynamic tilt angles).

In order to put these qualitative predictions on a more quantitative level, we performed reflectivity and absorbance calculations using the equations derived by Hansen *et al.*[32,33] and by Mielczarski *et al.*[27] The reflectivity R is calculated seperately for each component i of the incident light, *i.e.*, the s-polarized light (R_s), the tangential component of p-polarized light ($R_{p,t}$) and the normal component of p-polarized light ($R_{p,n}$). The quantity to be compared to the experimental data is the reflectivity difference ΔR, which is obtained by subtracting the reflectivity of the adsorbate covered substrate (R) from the reflectivity of the bare substrate (R^0) according to the following formula[27] (Fig. 4):

$$\Delta R_i(\Theta) = R_i^0(\Theta) - R_i(\Theta) = R_i^0(\Theta)/10^{\Delta A_i(\Theta)}$$

where

$$R_s^0(\Theta) = (|\xi_3(\Theta) - \xi_1(\Theta)/\xi_3(\Theta) + \xi_1(\Theta)|)^2$$

and

$$R_{pt}^0(\Theta) = R_{pn}^0(\Theta) = \left(\left|\left(\frac{\xi_3(\Theta)}{(n_3)^2} - \frac{\xi_1(\Theta)}{(n_1)^2}\right) \Big/ \left(\frac{\xi_3(\Theta)}{(n_3)^2} + \frac{\xi_1(\Theta)}{(n_1)^2}\right)\right|\right)^2$$

with

$$\xi_j(\Theta) = \sqrt{\left[(\hat{n}_j)^2 \cdot n_1 \cdot (\sin\Theta)^2\right]} \text{ and } \hat{n}_j = n_j + i \cdot k_j$$

and the absorbance ΔA

$$\Delta A_y(\Theta) = \frac{-16\pi}{\ln(10)} \cdot \left(\frac{\cos(\Theta)}{(n_3)^2 - 1}\right) \cdot \frac{n_2 \cdot k_2 \cdot d_2}{\lambda}$$

$$\Delta A_x(\Theta) = \frac{-16\pi}{\ln(10)} \cdot \left(\frac{\cos(\Theta)}{\left(\frac{(\xi_3(\Theta))^2}{(n_3)^4}\right) - (\cos(\Theta))^2}\right) \cdot \left[\frac{-(\xi_3(\Theta))^2}{(n_3)^4}\right]$$

$$\Delta A_z(\Theta) = \frac{-16\pi}{\ln(10)} \cdot \left(\frac{\cos(\Theta)}{\left(\frac{(\xi_3(\Theta))^2}{(n_3)^4}\right) - (\cos(\Theta))^2}\right) \times \left[\frac{-(\sin(\Theta))^2}{\left((n_2)^2 + (k_2)^2\right)^2}\right].$$

See Fig. 4 for the values of the refraction index n, the extinction coefficient k, and the thickness of the adsorbate layer d_2 used in the calculation of the change in reflectivity ΔR. The index j refers to the respective layer, *i.e.* the substrate, adsorbate or vacuum as indicated in Fig. 4.

The graph in Fig. 4 shows the calculated reflectivity difference for the frequency of the asymmetric carboxylate vibration (1617 cm^{-1}) as determined by the HREELS measurements.[7] The corresponding graph for the symmetric vibration at a frequency of 1340 cm^{-1} is virtually identical and therefore omitted here. These calculations allow us to go beyond the heuristic analysis considering only the TDM and predict not only the presence or absence of signals, but also their respective sign. Since the TDM of the asymmetric carboxylate vibration is orientated parallel to the surface along the [0001]-direction (see Fig. 1), ν_{as} interacts with p_t-light incident along the [0001] azimuth. This interaction results in a positive signal, because the reflectivity of p_t is positive at an incidence angle of 80°. The symmetric carboxylate vibration interacts with the normal component of the p-polarized light, which has negative reflectivity, and consequently gives rise to a negative signal. As both vibrations do not exhibit a TDM component in the [1$\bar{2}$10] direction, no signal is expected for s-polarized light incident along the [0001] azimuth. For light incident along the [1$\bar{2}$10] azimuth, the asymmetric carboxylate

vibration couples to the s-polarized light, yielding a negative signal (see Fig. 2b). The symmetric carboxylate vibration couples to the p_n-component, yielding a negative band as well (see also Fig. 2).

With knowledge about the sign of the vibrational bands resulting from the interaction between the transition dipole moments and the polarized light, we can also consider other plausible geometries for carbonates on ZnO(10$\bar{1}$0). An upright tridentate oriented along the [1$\bar{2}$10] direction is sketched in Fig. 5a along with the expected sign of the vibrational bands for s- and p-polarized light incident along the [0001] azimuth (left panel) and along the [1$\bar{2}$10] azimuth (right panel). For p-polarized light incident along the [0001] azimuth, only one negative band corresponding to the symmetric stretch vibration ν_s is expected. The corresponding TDM_s is orientated perpendicular to the surface and therefore interacts with the normal component of the p-polarized light, $E_{p,n}$. The asymmetric stretch vibration exhibits a TDM along the [1$\bar{2}$10] direction and hence cannot couple to p-polarized light incident along the [0001] azimuth. In contrast, s-polarized light incident along the [0001] azimuth can couple to the asymmetric stretch vibration ν_{as} leading to a corresponding peak in the spectrum. It cannot, however, couple to the TDM of the asymmetric stretch vibration oriented perpendicular to the surface. With the light incident along the [1$\bar{2}$10] azimuth, two peaks are predicted for p-polarization. As the TDM_{as} belonging to ν_{as} is now oriented in the same direction as the incident light, it can couple to the tangential component of the p-polarized light, $E_{p,t}$. This interaction leads to a positive band. The normal component $E_{p,n}$ couples to the asymmetric stretch vibration ν_{as} with its TDM_{as} oriented perpendicular to the surface, which leads to a negative band just as observed for the other azimuth. In this configuration, both the symmetric and the asymmetric stretch vibrations do not exhibit a TDM along the [0001] direction. Consequently, no signal is expected for s-polarized light.

A carboxylate species with the O–C–O backbone plane oriented along the [0001] direction and tilted by 45° towards the surface (*cf.* Fig. 5b) presents a more complicated case: while the TDM_{as} of the asymmetric stretch vibrations ν_{as} is oriented strictly along the [0001] direction, the TDM_s of the symmetric stretch vibration ν_s has a large component normal to the surface as well as along the [1$\bar{2}$10] direction. For light incident along the [0001] azimuth (*cf.* left panel in Fig. 5b), the p-polarized light can couple to both, the asymmetric and the symmetric vibrations; we expect a positive peak for the asymmetric stretch vibration ν_{as} coupling to the $E_{p,t}$ component and a negative peak for the symmetric stretch vibration ν_s interacting with the $E_{p,n}$ component, respectively. The s-polarized light can also couple to the component of the symmetric stretch vibration along the [1$\bar{2}$10] direction leading to a negative peak for light incident along the [0001] azimuth. For light incident along the [1$\bar{2}$10] azimuth, the E_s component can interact with the TDM_{as} of the asymmetric stretch vibration ν_{as}, which consequently shows up as a negative signal in the spectrum. The TDM_s of the symmetric stretch vibration can couple to both components of the p-polarized light, $E_{p,t}$ and $E_{p,n}$, and a signal is expected.

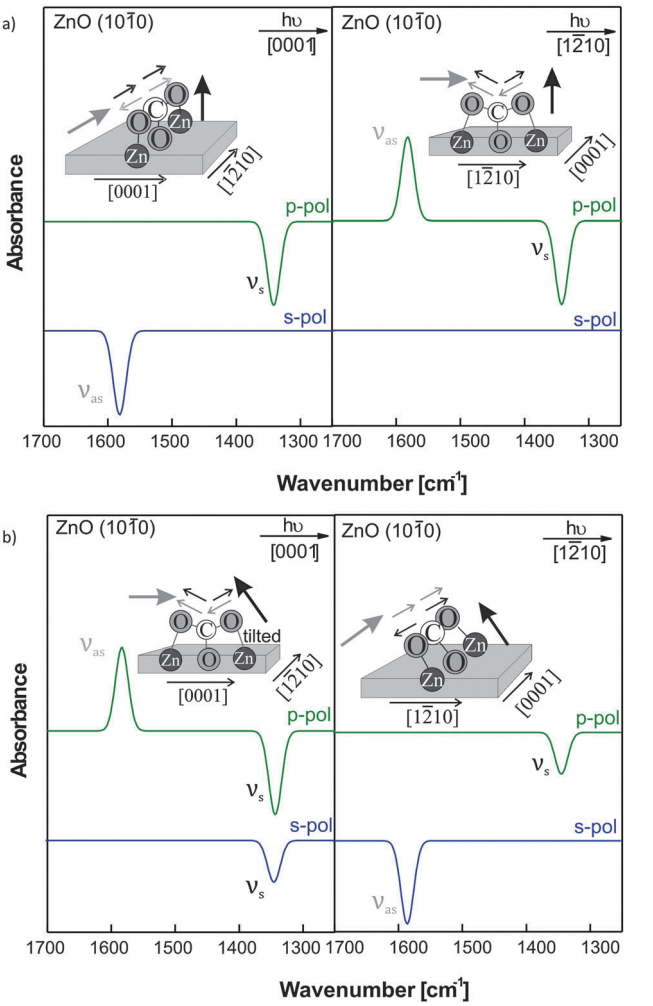

Fig. 5 Expected signals in IRRA spectra based on calculations for two different carbonate geometries: (a) a tridentate along the [1$\bar{2}$10]. (b) A tridentate oriented along the [0001] axis, but tilted towards the surface by 45°. Beam is incident along [0001] (left panels) and [1$\bar{2}$10] azimuth (right panels). The sketches show the different orientation of the tridentate on the surface, the arrows mark the movement during the vibration. The big black or grey arrows show the orientation of the transition dipole moment of the vibration.

This signal must be negative and smaller compared to the corresponding signal observed for the other azimuth as the prevailing negative band arising from the interaction with the $E_{p,n}$ component is reduced by the positive contribution arising from coupling to the $E_{p,t}$ component.

The predictions of the spectra obtained for the different adsorbate geometries as derived above demonstrate that only the adsorption geometry shown in Fig. 2 is compatible with our experimental data. Thus, the experimental data directly confirm the adsorption geometry proposed in an earlier publication which was derived from DFT calculations and NEXAFS experiments.[25] In particular, the IRRAS data present direct experimental evidence for the carboxylate exhibiting a negligible (static) tilt angle towards the surface.

The case of CO_2 adsorption on ZnO(10$\bar{1}$0) leading to the formation of carbonate species as reported above is markedly different from CO_2 adsorption on rutile TiO_2(110) as reported

Table 1 Comparison of the IRRAS results for CO_2 on ZnO(10$\bar{1}$0) with former data of vibrational spectroscopy or DFT calculations

Vibrational mode	HREELS	FTIR on ZnO particles	Our IRRAS results	DFT
ν_{as} (OCO)	1615[7]	1617,[9a] 1643,[9a] 1590,[9a] 1592,[9b] 1643,[9b] 1543[9b]	1584[c]/1591[d]	1562 (2 × 1)[25]
ν_{s} (OCO)	1340[7]	1343,[9a] 1295[9a]/1334,[9b] 1292[9b]	1340[c]/1344[d]	1291 (2 × 1)[25]

[a] At 100 K. [b] At RT. [c] Along [1$\bar{2}$10] azimuth. [d] Along [0001] azimuth.

by Lin *et al.*, where associative adsorption has been reported.[20] In this combined STM, IRRAS, TPD, and DFT study, the authors find CO_2 to adsorb in an essentially undistorted, linear form on two different sites. Bridging oxygen vacancies are the most stable adsorption sites, where the CO_2 molecule adopts a flat-lying geometry. After filling these sites, CO_2 starts to occupy 5-coordinated Ti^{4+} sites (Ti_{5c}). The resulting monodentate species is bound *via* one oxygen atom to individual Ti_{5c} with the O═C═O-axis tilted away from the surface normal.

In Fig. 2, we also provide a direct comparison between the IR-spectra recorded for ZnO powder particles in transmission at 100 K reported by Noei *et al.*[9] and our IRRAS data recorded for a ZnO(10$\bar{1}$0) single crystal. The powder particles used in this work had an average size of about 70 nm.[9] The powder spectra show a sharp ν_s absorption band at 1340 cm^{-1} (along with some minor contributions at smaller wavenumbers), whereas the ν_{as} band is substantially broadened and exhibits features at 1643 cm^{-1}, 1617 cm^{-1} and a shoulder at 1590 cm^{-1}. The frequency observed for the symmetrical carboxylate vibration agrees very well with the results presented here. In the case of the asymmetric carboxylate vibration, however, only the shoulder at 1590 cm^{-1} and not the much larger features observed on the powder particles is in good agreement with the signal in our data ascribed to the asymmetric carboxylate stretch vibration. Based on this comparison, we conclude that a number of species must be present on the powder particles which do not correspond to carboxylate species formed on a (10$\bar{1}$0) surface. This is an interesting and rather surprising observation, since these ZnO particles are reported to exhibit mainly ZnO(10$\bar{1}$0) facets accounting for more than 80% of their total surface area.[34] Such a dominance of ZnO(10$\bar{1}$0) facets would suggest that the strongest absorption peak on the particles should correspond to the absorption feature observed in our experiments on ZnO(10$\bar{1}$0), which is clearly not the case. In particular, this result is strikingly different from CO adsorption on ZnO particles and ZnO(10$\bar{1}$0) single crystals, where only a single sharp signal attributed to the CO stretch vibration on ZnO(10$\bar{1}$0) is found in the IR spectra recorded on ZnO particles.[35] In the carboxylate case, we feel unable to provide a more specific assignment of the two symmetric carboxylate vibrations at 1643 cm^{-1} and 1617 cm^{-1} on the ZnO particles. However, since the two features are found at higher wavenumbers in comparison to the ZnO single crystal, *i.e.* they are blue shifted, it can be speculated that they may correspond to carboxylate species bound to surface sites with higher Lewis acidity, *e.g.* the Zn-terminated (0001) surface or steps, edges, and similar defects. Such a behavior was found for CO on anatase particles.[36,37]

In Table 1, we have compiled peak positions of our IRRAS results to compare them with the corresponding peak positions obtained from HREELS, DFT-calculations and transmission powder spectra. The experimental data show reasonable agreement with the DFT calculations, which give slightly lower frequencies for both the symmetric and the asymmetric stretch vibration. The results from HREELS experiments on ZnO(10$\bar{1}$0) single crystals are in good agreement with our IRRAS data: the symmetric stretch vibration is detected at exactly the same frequency, while the asymmetric stretch vibration is found at slightly higher frequencies in the HREELS experiments. Given the limited resolution of HREELS, the results match very well. Overall, it is evident that our results are fully consistent with former vibrational measurements and calculations. The higher resolution of our data allows, however, us to draw important conclusions on the nature of the carboxylate species on the powder particles.

Conclusion

In conclusion, IRRAS data recorded for the tridentate carboxylate species on a single-crystal ZnO(10$\bar{1}$0) surface show a strong azimuthal and polarization dependence. To our knowledge, no IR-data have been recorded before for any ZnO single crystal surface. A detailed analysis of the data using a simple model accounting for the particular optical properties of dielectric surfaces yields a good agreement of the observed magnitudes and signs of the observed vibrational bands with a carboxylate species with its backbone plane oriented along the [0001] azimuth and perpendicular to the surface. A comparison of the high-resolution vibrational data to previously reported data for carboxylate species adsorbed on ZnO powders allows us to conclude that on the ZnO nanoparticles the carboxylates are predominantly not bound to (10$\bar{1}$0) facets – which according to TEM microscopic studies form about 80% of the surface area,[34] but must be bound to different sites, *e.g.* steps, vacancies or other defects.

Acknowledgements

The financial support from Science and Technology of Nanosystems program (Karlsruhe Institute of Technology) is gratefully acknowledged. M.B. acknowledges the Helmholtz Research School ''Energy-related catalysis'' and F.B. acknowledges the Alexander von Humboldt Foundation for financial support.

Notes and references

1 C. F. Klingshirn, *Zinc Oxide: From Fundamental Properties Towards Novel Applications*, Springer, Heidelberg, 2010.
2 C. Jagadish and S. J. Pearton, *Zinc Oxide Bulk, Thin Films And Nanostructures: Processing, Properties And Applications*, Elsevier Science & Technology Books, 2006.

3 H. Morkoc and Ü. Özgür, *Zinc Oxide: Fundamentals, Materials and Device Technology*, Wiley, 2008.
4 E. Martono, M. P. Hyman and J. M. Vohs, *Phys. Chem. Chem. Phys.*, 2011, **13**, 9880–9886.
5 J. B. Hansen and P. E. Højlund Nielsen, *Handbook of Heterogeneous Catalysis*, Wiley-VCH Verlag GmbH & Co. KGaA, 2008.
6 S. Schenk, J. Notni, U. Köhn, K. Wermann and E. Anders, *Dalton Trans.*, 2006, 4191–4206.
7 Y. Wang, R. Kováčik, B. Meyer, K. Kotsis, D. Stodt, V. Staemmler, H. Qiu, F. Traeger, D. Langenberg, M. Muhler and C. Wöll, *Angew. Chem., Int. Ed.*, 2007, **46**, 5624–5627.
8 Y. Wang, X. Xia, A. Urban, H. Qiu, J. Strunk, B. Meyer, M. Muhler and C. Wöll, *Angew. Chem., Int. Ed.*, 2007, **46**, 7315–7318.
9 H. Noei, C. Wöll, M. Muhler and Y. Wang, *J. Phys. Chem. C*, 2011, **115**, 908–914.
10 F. Voigts, F. Bebensee, S. Dahle, K. Volgmann and W. Maus-Friedrichs, *Surf. Sci.*, 2009, **603**, 40–49.
11 E. Kadossov and U. Burghaus, *J. Phys. Chem. C*, 2008, **112**, 7390–7400.
12 J. Suzanne, V. Panella, D. Ferry and M. Sidoumou, *Surf. Sci.*, 1993, **293**, L912–L916.
13 O. Seiferth, K. Wolter, B. Dillmann, G. Klivenyi, H. J. Freund, D. Scarano and A. Zecchina, *Surf. Sci.*, 1999, **421**, 176–190.
14 H. Kuhlenbeck, C. Xu, B. Dillmann, M. Hassel, B. Adam, D. Ehrlich, S. Wohlrab, H. J. Freund, U. A. Ditzinger, H. Neddermeyer, M. Neuber and M. Neumann, *Ber. Bunsen-Ges.*, 1992, **96**, 15–27.
15 Y. Wang, A. Lafosse and K. Jacobi, *J. Phys. Chem. B*, 2002, **106**, 5476–5482.
16 H. Y. Wang and W. F. Schneider, *Phys. Chem. Chem. Phys.*, 2010, **12**, 6367–6374.
17 J. A. Hinojosa, A. Antony, C. Hakanoglu, A. Asthagiri and J. F. Weaver, *J. Phys. Chem. C*, 2012, **116**, 3007–3016.
18 M. A. Henderson, *Surf. Sci.*, 1998, **400**, 203–219.
19 T. L. Thompson, O. Diwald and J. T. Yates, *J. Phys. Chem. B*, 2003, **107**, 11700–11704.
20 X. Lin, Y. Yoon, N. G. Petrik, Z. J. Li, Z. T. Wang, V. A. Glezakou, B. D. Kay, I. Lyubinetsky, G. A. Kimmel, R. Rousseau and Z. Dohnalek, *J. Phys. Chem. C*, 2012, **116**, 26322–26334.
21 J. Kattner and H. Hoffmann, *Handbook of Vibrational Spectroscopy*, John Wiley & Sons, Ltd, 2006.
22 A. Gutiérrez-Sosa, S. Crook, S. Haq, R. Lindsay, A. Ludviksson, S. Parker, C. T. Campbell and G. Thornton, *Faraday Discuss.*, 1996, **105**, 355–368.
23 V. Schott, H. Oberhofer, A. Birkner, M. Xu, Y. Wang, M. Muhler, K. Reuter and C. Wöll, *Angew. Chem., Int. Ed.*, 2013, **52**, 11925–11929.
24 C. Wöll, *Prog. Surf. Sci.*, 2007, **82**, 55–120.
25 K. Kotsis, D. Stodt, V. Staemmler, R. Kovacik, B. Meyer, F. Traeger, D. Langenberg, T. Strunskus, M. Kunat and C. Wöll, *Z. Phys. Chem.*, 2008, **222**, 891–915.
26 R. Davis, J. F. Walsh, C. A. Muryn, G. Thornton, V. R. Dhanak and K. C. Prince, *Surf. Sci.*, 1993, **298**, L196–L202.
27 J. A. Mielczarski and R. H. Yoon, *J. Phys. Chem.*, 1989, **93**, 2034–2038.
28 M. C. Xu, H. Noei, K. Fink, M. Muhler, Y. M. Wang and C. Wöll, *Angew. Chem., Int. Ed.*, 2012, **51**, 4731–4734.
29 S. G. Gil Girol, T. Strunskus, M. Muhler and C. Wöll, *J. Phys. Chem. B*, 2004, **108**, 13736–13745.
30 R. G. Greenler, *J. Chem. Phys.*, 1966, **44**, 310–315.
31 R. G. Greenler, D. R. Snider, D. Witt and R. S. Sorbello, *Surf. Sci.*, 1982, **118**, 415–428.
32 W. N. Hansen, *J. Opt. Soc. Am.*, 1968, **58**, 380–388.
33 W. N. Hansen, *Symp. Faraday Soc.*, 1970, **4**, 27–35.
34 D. Scarano, G. Spoto, S. Bordiga, A. Zecchina and C. Lamberti, *Surf. Sci.*, 1992, **276**, 281–298.
35 H. Noei, C. Wöll, M. Muhler and Y. M. Wang, *Appl. Catal., A*, 2011, **391**, 31–35.
36 L. Mino, G. Spoto, S. Bordiga and A. Zecchina, *J. Phys. Chem. C*, 2012, **116**, 17008–17018.
37 C. Deiana, G. Tabacchi, V. Maurino, S. Coluccia, G. Martra and E. Fois, *Phys. Chem. Chem. Phys.*, 2013, **15**, 13391–13399.
38 R. C. Weast, *CRC handbook of chemistry and physics*, CRC Press, Boca Raton, FL, 62nd edn, 1981–1982.
39 R. J. Gonzalez, R. Zallen and H. Berger, *Phys. Rev. B: Condens. Matter Mater. Phys.*, 1997, **55**, 7014–7017.

